ECCOMAS Congress 2016
VII European Congress on Computational Methods in Applied Sciences and Engineering
M. Papadrakakis, V. Papadopoulos, G. Stefanou, V. Plevris (eds.)
Crete Island, Greece, 5–10 June 2016

VALIDATION OF MODELING ASSUMPTIONS FOR THE BUILDUP SIMULATION OF LASER BEAM MELTING ON THE BASIS OF THE RESIDUAL STRESS DISTRIBUTION

F. Bayerlein[1], C. Zeller[1], M. Wunderer[1], J. Weirather[1], M. Schmid[1], C. Seidel[1], M. F. Zaeh[1], R. Hessert[2], G. Schlick[2], T. Uihlein[2], and M. Hofmann[3]

[1]Technical University Munich
Institute for Machine Tools and Industrial Management
Boltzmannstraße 15, 85748 Garching, Germany
e-mail: fabian.bayerlein@iwb.tum.de

[2] MTU Aero Engines AG
Dachauer Straße 665, 80995 Munich, Germany
e-mail: roland.hessert@mtu.de

[3] Heinz Maier-Leibnitz Zentrum (MLZ)
Technical University Munich
Lichtenbergstraße 1, 85748 Garching, Germany
e-mail: michael.hofmann@frm2.tum.de

Keywords: Laser beam melting, computational methods, engineering sciences, neutron diffraction, X-ray diffraction, residual stresses

Abstract. *The growing market for additive manufacturing processes such as laser beam melting (LBM) poses new challenges. With more difficult product requirements, the need for a deeper understanding of the resulting stress states and the underlying physical principles increases. To gain a deeper understanding of the residual stress states of LBM-manufactured parts, simulations of the build-up process were carried out and validated by means of neutron diffraction (ND), X-ray diffraction (XRD) as well as incremental hole-drilling (IHD). The gathered data is also intended to serve as a validation case for other simulation models and tools.*

1 Introduction

Laser beam melting is an additive manufacturing technique to produce dense metal parts through layer-wise powder melting and re-solidification by means of a focused laser beam. This leads to significant temperature gradients both spatially and temporally, which in turn cause residual stresses through thermal strains. Today, the knowledge about the correlation between part geometry, resulting temperature gradients during the manufacturing process and, ultimately, residual stress states after the end of the build process is not sufficient and only partly validated [1, 2]. This issue is a considerable challenge for the component design of dimensionally accurate parts [3, 4]. Currently, a lot of process know-how and expert knowledge is necessary to pre-warp the geometry in such a way that the manufactured result matches the target geometry. An iterative approach to meet this challenge before the manufacturing stage by pre-warping the geometry based on simulation results is described in [5]. In recent time, further simulation models have been increasingly developed to predict residual stresses and distortions of additively manufactured parts [6, 7, 8, 9, 10].
This paper presents the validation results of the simulation model described in [5, 11]. Moreover, to create a general understanding of the correlation between temperature gradients and residual stresses in LBM, a simple cuboid geometry was selected. The presented investigations focus on the nickel-base superalloy Inconel 718, which is highly relevant to e. g. the aerospace industry [12, 13]. Validation of the simulation model was already carried out for both a tool steel 1.2709 [14] and the AlSi12 material system [15].

Neutron diffraction measurements of a massive cuboid geometry were used in order to understand the stress state within the bulk volume. In addition, incremental hole-drilling as well as X-ray diffraction measurements were carried out to validate residual stresses close to the surface. An alternative approach to estimate residual stresses in the interior of additively manufactured parts using digital image correlation is presented in [2]. A more in-depth analysis of the microstructure and mechanical behavior of Inconel 718 fabricated by selective laser melting is described in [16, 17]. Additional details about the experiments are summarized in Subsection 2.1.

For the simulation presented in this manuscript, the LBM process is simulated by a sequentially coupled finite element simulation of the thermal and thermomechanical processes. Due to the complexity of the real process, simplifications are necessary for the simulation to calculate residual stresses and distortions on the scale of industry relevant parts within a reasonable time frame. While real parts comprise thousands of layers consisting of thousands of hatches, several of those layers are combined into so-called layer compounds for the simulation [18]. Furthermore, a simultaneous heat input to the whole layer is used, thereby neglecting the distortions and residual stresses caused by the single weld seams [11]. Subsection 2.2 contains additional information on the used simulation model.

2 Methodology

The presented results are intended to help to understand the distribution of residual stresses in a simple additively manufactured cuboid structure in order to improve the understanding and to serve as a way of validating the results of corresponding simulations. The necessary experimental methods and analyses are presented in this section as well as the simulation model that is to be validated.

2.1 Experimental setup and methods

The geometry used for the validation is shown in Figure 1. Specimen manufacturing was carried out on an EOS Eosint M280 LBM machine calibrated and maintained for aerospace production use located at MTU Aero Engines AG in Munich. The machine uses a $400\,\mathrm{W}$ Nd:YAG fiber laser with a spot size of approximately $80\,\mu\mathrm{m}$. Laser focusing and positioning is achieved by an F-Theta lens and two Galvanometer scanning mirrors. Argon was used as a shielding gas and the oxygen concentration within the build chamber is controlled to a maximum of $0.1\,\%$.

The powder material for the experiments was Inconel 718 with a particle diameter between $15\,\mu\mathrm{m}$ and $45\,\mu\mathrm{m}$ provided by Oerlikon Metco. The EOS standard parameter set for this material and $20\,\mu\mathrm{m}$ layer thickness originally developed for the Eosint M270 generation was used. This includes, among others, a stripe pattern for the exposure strategy.

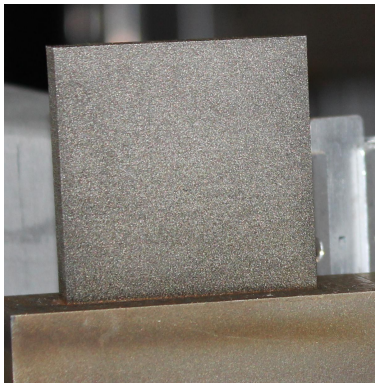

(a) Specimen on build plate within the experimental setup

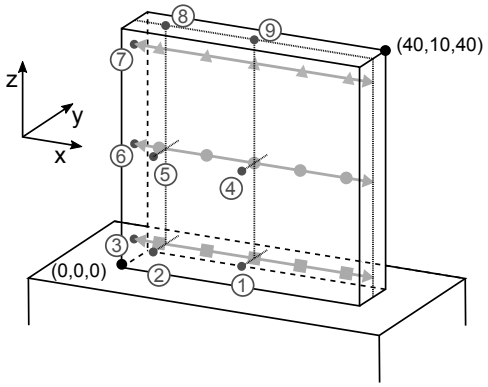

(b) Schematic depiction of the cuboid geometry with the build plate. The lines with markers represent the location for the neutron diffraction measurements, while the numbered dots indicate the location of X-ray and hole-drilling measurements.

Figure 1: The used specimen, a cuboid geometry ($40 \times 40 \times 10\,\mathrm{mm}^3$). The directions are referred to in the following as x: longitudinal, y: transversal and z: normal.

IHD and XRD techniques were applied in side and top surfaces of an LBM manufactured cuboid sample to characterize the residual stress depth distributions. For the IHD technique, high-speed drilling equipment was used to perform a cylindrical blind hole. This technique is recommended since minor drilling-induced plastic deformations occur and a satisfying hole shape can be achieved. Surface strain relief was measured by three-element strain gage rosettes (CEA-06-062UM-120, Measurements Group) in depth increments of 0.02 to $0.06\,\mathrm{mm}$, up to about $1.2\,\mathrm{mm}$ below the surface. Smaller steps were carried out close to the surface to access stress gradients more precisely. The typical hole diameter was about $1.9\,\mathrm{mm}$. Residual stress evaluation was carried out according to the differential method, using the elastic constants $E = 190\,\mathrm{GPa}$ and $\nu = 0.34$ for the top surface and $E = 175\,\mathrm{GPa}$ and $\nu = 0.34$ for the side surfaces of the rectangular sample.

XRD residual stress analysis was combined with local electrolytic layer removal to obtain residual stress profiles. Stress relaxation due to layer removal was neglected since the affected region was small and no significant relaxation effects could be expected. Lattice deformations of the Ni planes were measured on a modified ψ-diffractometer (Xstress 3000 G2, Stresstech Group) for 13 ψ-angles between $-45°$ and $45°$ using Mn Kα radiation. Residual stresses were calculated for the plain stress condition using the X-ray elastic constants $E\,\{311\} = 199\,\mathrm{GPa}$

and $\nu\{311\} = 0.33$ for IN718 matrix material [19]. In addition to the macroscopic residual stresses, the full width at half maximum (FWHM) values of the X-ray diffraction peaks were also recorded; they indicate near surface microstructural changes in the material due to the LBM process.

The neutron diffraction measurements were performed at the STRESS-SPEC instrument. For the neutron diffraction experiment a wavelength of $\lambda = 1.55\,\text{Å}$ was selected using the Si (400) monochromator, which allowed to measure the Nickel $\{311\}$ reflection at a scattering angle of about $2\theta_S \approx 91°$. The gauge volume was defined using a $2 \times 2\text{mm}^2$ slit in the incoming beam and a radial collimator having a $2\,\text{mm}$ field of view in the diffracted beam. In total three lines at half width ($y = 5\,\text{mm}$) of the block and at different positions (e. g. at $z = 5\,\text{mm}$, $z = 20\,\text{mm}$ and $z = 38\,\text{mm}$) along the build direction z were measured (cf. Figure 1b on the preceding page). Each line consisted of five measurement positions along the long axis of the IN718 block with the exact positions in the x-direction at $2\,\text{mm}$, $12\,\text{mm}$, $20\,\text{mm}$, $28\,\text{mm}$ and $38\,\text{mm}$, respectively.

The strain is measured in the direction of the scattering vector, which bisects the incident and the diffracted beam. Since stress is a tensor, measurements are generally required in six orientations to completely determine the stress state at any point in the sample. However, in case of the built IN718 cuboid, we inferred that the principal stress axes roughly coincide with the principal axes x, y and z of the cuboid. Additionally, the effect of assuming the principal stresses is not relevant for the comparisons carried out in this study, as the stresses in three perpendicular directions are correctly gathered, they may just not account for all of the stress in the sample [20]. As the main goal of this study is the validation of a simulation model and more exactly, the stresses along the principal axes of the cuboid geometry, no systematical error is introduced. Thus, the stresses can be calculated from the measured strains using diffraction elastic constants $E\{311\}$ and $\nu\{311\}$.

As in our case no stress free reference sample was available, the stresses were calculated using the mechanical boundary condition that the near surface stresses in x-direction should decline to zero. The possible error of this assumption relates to a shift in the y-axis of the plots in Figure 3 on page 7 but is not depicted in the plots.

2.2 Simulation

The used simulation model was developed at the Institute for Machine Tools and Industrial Management (*iwb*) and contains several modeling assumptions necessary to allow the simulation of the highly complex laser beam melting process (cf. [5, 11] for additional details).
The position of the nodes of the computational mesh, for example, is required to be restricted to discrete levels in build-up direction, similar to the real layer wise manufacturing process. With real parts comprising thousands of layers, abstractions are made by summarizing multiple real layers in so-called layer compounds. Modeling every single layer in the simulation would currently result in an unacceptably long calculation time. It is however not considered necessary due to the fact that the layers close to each other share the same temperature history and are therefore subject to similar thermal loading and thus expected to exhibit similar mechanical loading. The presented results were generated with a layer compound height of $0.5\,\text{mm}$ and hexahedral elements of similar size.

The simulation uses a simultaneous heat input to the whole layer and considers the effect of the heat conduction through the part, neglecting stresses introduced by the single weld seams. While the selective solidification leads to high initial stresses, considering the established subsequent manufacturing process, where multiple layers are remelted and hatch patterns are rotated

between each layer, the effect is assumed to be characterizable by a homogeneous heat input as a first step.

The heat input is realized by adjusting the temperature of the nodes on the upside of the top layer to solidus temperature. The load time corresponds to the time a point in the real process is subject to temperatures above solidus and is based on Rosenthal's solution for a moving heat source on a semi-infinite body [21].

The thermal and mechanical simulation are sequentially coupled by solving the transient heat equation and applying the calculated temperature distribution per time step as distinct load steps within the mechanical simulation. The feedback, the resulting warpage, is deemed negligible for the thermal simulation due to its limited effect size in the range of $10^{-4}\,\mathrm{m}$. As distortions of the building platform are observable in the real manufacturing process, it is necessary to take the building platform into account. The model thus not only comprises the part but also an exact representation of the used building platform.

In order to validate the simulation, a comparison of values of residual stresses was carried out.

3 Results

Post-process light and scanning electron microscopic images reveal the expected dense structure with columnar grains in the x-y-plane [16, 17] (cf. Fig. 2). In contrast, the x-z-plane of the part shows no predominant direction in terms of grain orientation (cf. Figure 2b on the following page).

The results of the different stress evaluations are depicted in Figure 3 on page 7 and Figure 4 on page 8. The first three plots show a comparison between the simulated and the measured stresses in the three principal directions of the cuboid geometry, along the measurement paths of the neutron diffraction measurements with the hollow markers indicating experimentally gathered values. The given error is limited to the propagation of the fitting error inherent to diffraction measurements, i. e. the error from choosing the correct reference sample for the stress-free lattice strain is not included. All errors are acceptable, with the transversal stresses exhibiting the highest uncertainty.

The plot for the normal stresses shows similar tendencies for all measurement paths, the respective magnitude is however overestimated by the simulation for the inner lower area of the part. In the border areas, tensile stresses near yield are both simulated and measured while the middle of the part is exhibiting compressive stresses that decline with the distance from the build plate. Both the simulation and the measurement suggest an almost neutral stress state along the upper path with the simulation predicting tensile stresses near the surface.

The longitudinal stresses exhibit the best agreement between simulation and measurements. With the exception of the central point of the middle path, the simulation results are within or close to the given experimental accuracy. The stress distribution is characterized by a low level of tensile stresses near the bottom of the part, a similar level of compressive stresses along the path at $z = 20\,\mathrm{mm}$ and a maximum at the top and in the middle of the part, exhibiting tensile stress. The boundary condition, that longitudinal stresses should disappear at the edge of the geometry in x-direction, was used to set the stress-free reference angle. Thus, the respective values naturally decline towards $x = 0$ and $x = 40\,\mathrm{mm}$.

In the transversal, i. e. the y-direction, the predicted stresses follow a similar trend as the measurements, the agreement is however not sufficient, especially for the lowest scan path in the middle of the part. Additionally, the missing symmetry in combination with the high expected gradients suggests a positioning error of the gauge volume for one of the extreme

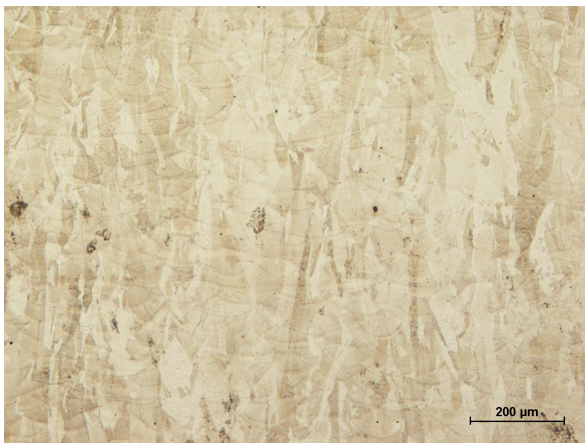

(a) Light microscope image of the x-z-plane, etched and 100 times magnified

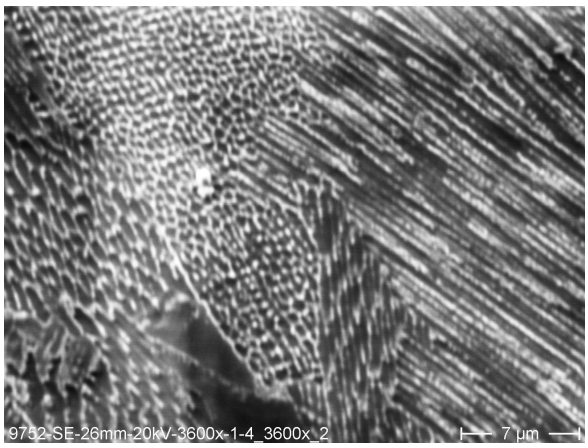

(b) Scanning electron microscopic image of the x-z-plane, etched and 3600 times magnified

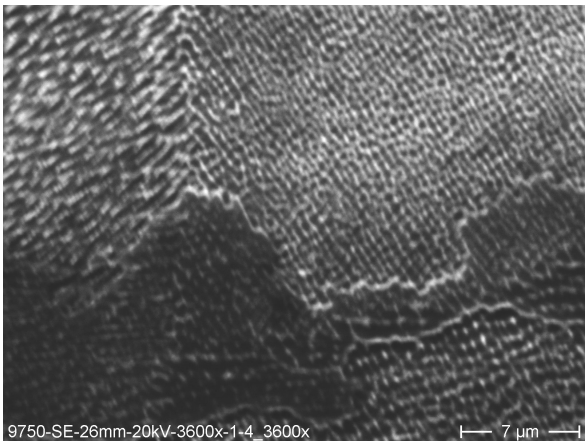

(c) Scanning electron microscopic image of the x-y-plane, etched and 3600 times magnified

Figure 2: Microstructure of the used specimen

positions ($x = 2$ or $x = 38\,\mathrm{mm}$). The stresses are rather negligible in the middle of the part but exhibit a considerable maximum of $300\,\mathrm{MPa}$ near the edge and bottom of the part.

The contour plots in Figure 4 on page 8 combine all determined values for an easier comparison. The plots are stretched to show a quadratic cross section to increase readability, with only Figure 4f having the original aspect ratio. The contour lines represent the results of the simulation described in Subsection 2.2, the values marked with a diamond indicate neutron diffraction results and the alphanumerically labeled data, marked by circles and rectangles, was provided by the IHD and XRD experiments. For most measuring points, the results of the last two methods (obtained at corresponding positions on opposite sides of the cuboid) coincide, but especially for holes close to edges of the cuboid, IHD measurements are less reliable and diverge from those of the XRD trials due to plastic deformation. In these cases, the results obtained by X-ray diffraction are used and the corresponding points are marked with a rectangle instead of a circle. Additionally, if the cross sections do not coincide with actual measurement points, a linear interpolation between the neighboring points is used. For example, no neutron diffraction result is available for the cross section at $x = 5$ and thus it is inferred from the values at $x = 2$ and $x = 11$.

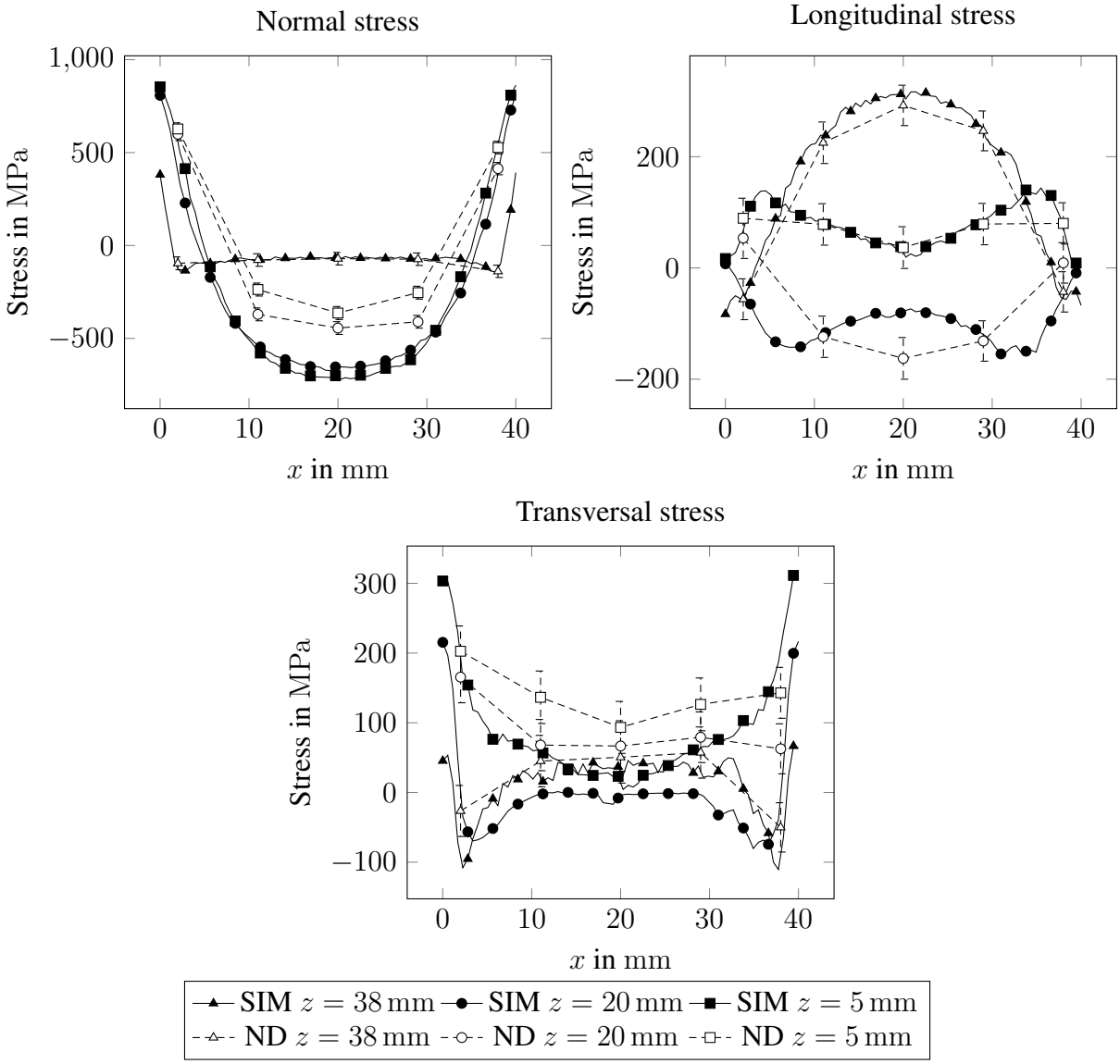

Figure 3: Comparison of simulated (SIM) and measured stresses by neutron diffraction (ND) for the three principal directions of the geometry in different build-up (z) heights

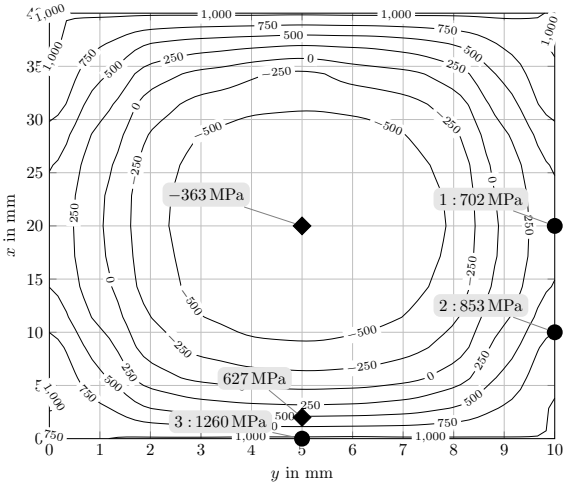

(a) Normal stresses at $z = 5\,\mathrm{mm}$

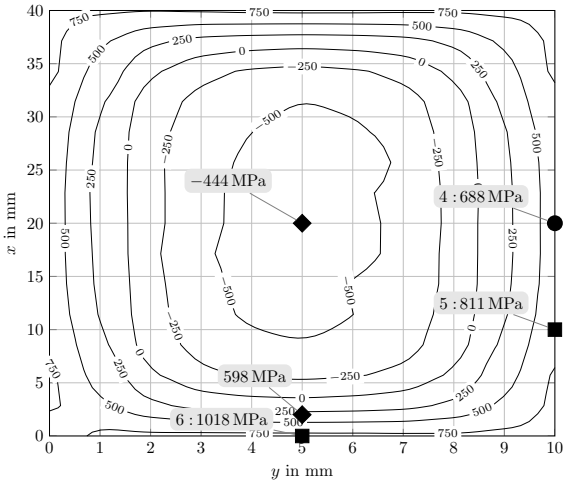

(b) Normal stresses at $z = 20\,\mathrm{mm}$

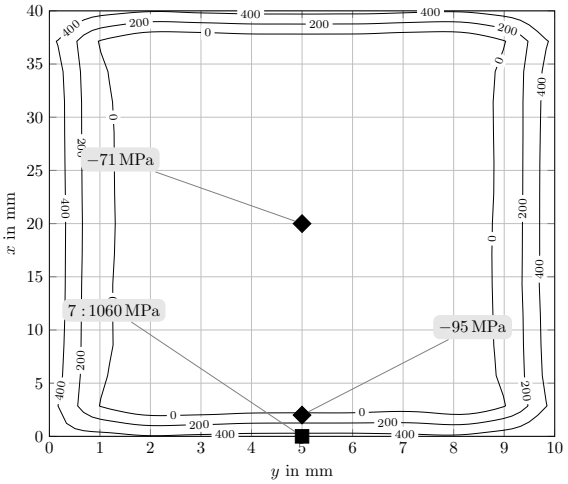

(c) Normal stresses at $z = 38\,\mathrm{mm}$

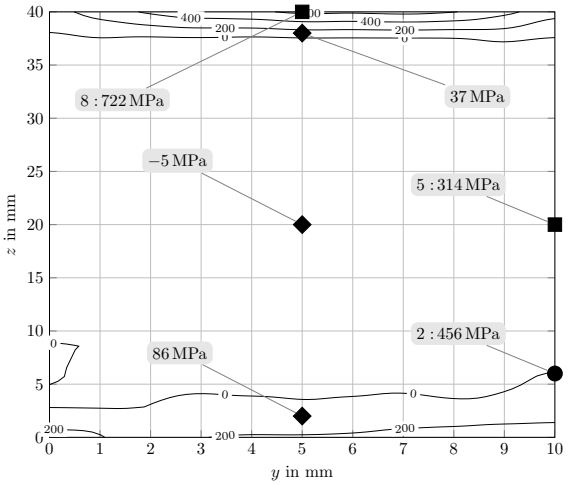

(d) Longitudinal stresses at $x = 5\,\mathrm{mm}$

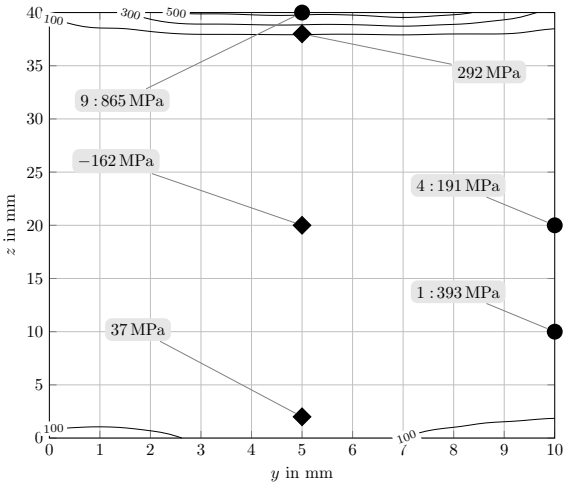

(e) Longitudinal stresses at $x = 20\,\mathrm{mm}$

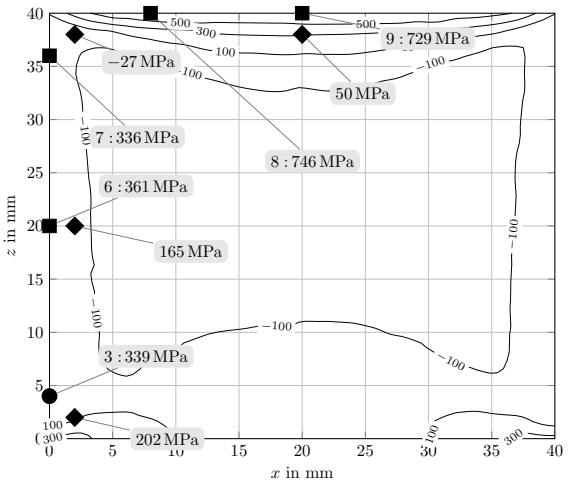

(f) Transversal stresses at $y = 5\,\mathrm{mm}$

Figure 4: Comparison of simulated (contour plot), neutron diffraction (diamonds), IHD (circle) as well as XRD (rectangle) measured results for the residual stresses in the presented cuboid geometry. The lines in the contour plots are equidistant.

The stress plots for the z-direction show the mentioned characteristic of high tensile stresses in the areas close to the surface and a compressive region in the middle of the part that declines with increasing z-height (cf. Figures 4a to c). The experimental results match the trend and show acceptable agreement with the simulation. However, the magnitude of tensile stresses found by experiments is not reproduced by the simulation, e. g. Figure 4c, measurement point 7.

In the longitudinal x-direction, the plots continue to show the agreement between ND and simulation. However, the high tensile stresses in the regions close to the surface are not predicted by the simulation. Additionally, the plot exhibits a certain level of asymmetry. This is attributable to the non-symmetric placement of the cuboid on the build plate.

For the transversal stresses, the agreement is less prominent. While the high stresses at the top of the part are correctly predicted, the simulation results do not match the experiment in the side surfaces of the cuboid. The stress state is characterized by tensile stresses at the bottom and top of the part and a compressive region in the middle of the upper half of the geometry.

4 Discussion and Conclusion

The prediction of residual stresses shows sufficient agreement with the measured values. However, especially in the border areas, the prediction and experiment differ from one another. This is assumed to be attributable to the missing modeling of the contour exposure.

The prediction of normal stresses shows an overestimation of the actual result. This is related to the modeling of the heat input that, in contrast to the real process, only accounts for a heat flow in z-direction as the consecutive hatches are summarized, eliminating temperature gradients in the x-y-area of the topmost layer. The further development should aim to incorporate the effects of the hatching into the simulation model and solve this issue.

However, the level of agreement between simulation and neutron diffraction results is highly encouraging and suggests that the chosen modeling approach is suitable for the simulation of the process. The conclusions are in particular:

1. The stresses occurring in an LBM-manufactured cuboid range from high tensile areas near yield close to the surface of the part to medium compressive stresses in the middle.
2. The presented simulation tool is capable of predicting the trend of residual stresses for the cuboid geometry.
3. The main point of deviation is the area close to the surface that exhibits very high tensile stresses not predicted by the simulation.

5 Outlook

Further investigations are necessary that include measurements of the stresses within the build plate in order to get a complete picture of the stress distribution. The statistical power of the work carried out is very low as only one sample part manufactured on one LBM system with one scan strategy was examined. The representativeness of the results is to be examined. It is however expected, that the results of other manufacturing systems are comparable. Additionally, the stripe pattern is one example of a heat input that is as homogeneous as possible, comparable to the also well-established chessboard strategy, and may thus serve as a valid reference point for this kind of strategy. Last, further studies should combine results of warpage and residual stresses so that the full mechanical response to the manufacturing process becomes available.

6 Acknowledgments

The research leading to these results has received funding from the European Union's Seventh Framework Program (FP7/2007-2013) for the Clean Sky Joint Technology Initiative under grant agreement No. 287087. However, explanations made reflect only the authors' views. Hence, the JU and the Union are not liable for any use that may be made of the information contained therein. The IGF-Project No 17.911 N / DVS-No. 13.007 was promoted by the AiF under the program for the promotion of industrial research and development (IGF) by the Federal Ministry of Economics and Technology. This work is based upon experiments performed at the STRESS-SPEC instrument operated by FRM II at the Heinz Maier-Leibnitz Zentrum (MLZ), Garching, Germany.

References

[1] Terry T. Wohlers. *Wohlers report 2014. 3D printing and additive manufacturing state of the industry annual worldwide progress report*. Fort Collins, Col.: Wohlers Associates, 2014. 276 pp. ISBN: 9780991333202.

[2] Amanda S. Wu et al. "An Experimental Investigation into Additive Manufacturing-Induced Residual Stresses in 316L Stainless Steel". In: *Metallurgical and Materials Transactions A* 45 (13 2014), pp. 6260–6270. ISSN: 1073-5623. DOI: 10.1007/s11661-014-2549-x.

[3] William E. Frazier. "Metal Additive Manufacturing: A Review". English. In: *Journal of Materials Engineering and Performance* 23 (6 2014), pp. 1917–1928. ISSN: 1059-9495. DOI: 10.1007/s11665-014-0958-z. URL: http://dx.doi.org/10.1007/s11665-014-0958-z.

[4] J.-P. Kruth et al. "Assessing and comparing influencing factors of residual stresses in selective laser melting using a novel analysis method". In: *Proceedings of the Institution of Mechanical Engineers, Part B: Journal of Engineering Manufacture* 226 (6 2012), pp. 980–991. ISSN: 0954-4054. DOI: 10.1177/0954405412437085.

[5] F. Bayerlein et al. "Improving cost effectiveness in additive manufacturing – Increasing dimensional accuracy in laser beam melting by means of a simulation-supported process chain". In: *Conference proceedings / Die Fachkonferenz zur Numerischen Simulation*. CADFEM GmbH et al. Grafing bei München, Darmstadt: CADFEM GmbH, 2015, pp. 1–9. ISBN: 393752312X.

[6] Nils Keller and Vasily Ploshikhin. "New Method for fast predictions of residual stress and distortion of AM parts". In: *Proceedings of the 25th Solid Freeform Fabrication Symposium*. Ed. by D. L. Bourell et al. Vol. 25. The University of Texas at Austin. Austin, TX and USA, 2014, pp. 1229–1237.

[7] Richard Martukanitz et al. "Toward an integrated computational system for describing the additive manufacturing process for metallic materials". In: *Additive Manufacturing* 1-4 (2014), pp. 52–63. ISSN: 22148604. DOI: 10.1016/j.addma.2014.09.002.

[8] Loucas Papadakis et al. "A computational reduction model for appraising structural effects in selective laser melting manufacturing". In: *Virtual and Physical Prototyping* 9 (1 2014), pp. 17–25. ISSN: 1745-2759. DOI: 10.1080/17452759.2013.868005.

[9] Nachiket Patil. *A novel numerical framework for simulation of multiscale spatio-temporally non-linear systems in additive manufacturing processes*. 2014. DOI: 10.18297/etd/1099.

[10] W. King et al. "Overview of modelling and simulation of metal powder bed fusion process at Lawrence Livermore National Laboratory". In: *Materials Science and Technology* 31 (8 2015), pp. 957–968. ISSN: 0267-0836. DOI: 10.1179/1743284714Y.0000000728.

[11] C. Seidel et al. "Simulation of the Laser Beam Melting Process – Approaches for an Efficient Modelling of the Beam-material Interaction". In: *Procedia CIRP* 25 (2014), pp. 146–153. ISSN: 22128271. DOI: 10.1016/j.procir.2014.10.023.

[12] A. Thomas et al. "High temperature deformation of Inconel 718". In: *Journal of Materials Processing Technology* 177 (1-3 2006), pp. 469–472. ISSN: 09240136. DOI: 10.1016/j.jmatprotec.2006.04.072.

[13] Fritz Klocke et al. "Turbomachinery component manufacture by application of electrochemical, electro-physical and photonic processes". In: *CIRP Annals - Manufacturing Technology* 63 (2 2014), pp. 703–726. ISSN: 0007-8506. DOI: 10.1016/j.cirp.2014.05.004.

[14] Michael F. Zaeh and Gregor Branner. "Investigations on residual stresses and deformations in selective laser melting". In: *Production Engineering* 4 (1 2010), pp. 35–45. ISSN: 0944-6524. DOI: 10.1007/s11740-009-0192-y.

[15] T. A. Krol et al. "Verification of Structural Simulation Results of Metal-based Additive Manufacturing by Means of Neutron Diffraction". In: *Physics Procedia* 41 (2013), pp. 849–857. ISSN: 18753892. DOI: 10.1016/j.phpro.2013.03.158.

[16] K. N. Amato et al. "Microstructures and mechanical behavior of Inconel 718 fabricated by selective laser melting". In: *Acta Materialia* 60 (5 2012), pp. 2229–2239. ISSN: 13596454. DOI: 10.1016/j.actamat.2011.12.032.

[17] Johannes Strößner, Michael Terock, and Uwe Glatzel. "Mechanical and Microstructural Investigation of Nickel-Based Superalloy IN718 Manufactured by Selective Laser Melting (SLM)". In: *Advanced Engineering Materials* 17 (8 2015), pp. 1099–1105. ISSN: 1527-2648. DOI: 10.1002/adem.201500158.

[18] G. Branner. *Modellierung transienter Effekte in der Struktursimulation von Schichtbauverfahren*. Vol. 246. Forschungsberichte / IWB. München: Utz, Herbert, 2011. 230 S. ISBN: 3831640718.

[19] Julia N. Repper. "Einfluss mikroskopischer Eigenspannungen auf die makroskopische Eigenspannungsanalyse mittels Neutronenbeugung". Dissertation. München: Technische Universität München, 2010-01-01.

[20] R. A. Winholtz and A. D. Krawitz. "The effect of assuming the principal directions in neutron diffraction measurement of stress tensors". In: *Materials Science and Engineering: A* 205 (1–2 1996), pp. 257–258. ISSN: 09215093. DOI: 10.1016/0921-5093(95)10040-7.

[21] D. Rosenthal. "Mathematical theory of heat distribution during welding and cutting". In: *Welding Journal* 5 (20 1941), pp. 220–234.